A NOVEL CONFIGURATION OF A DUAL CONCENTRATED PHOTOVOLTAIC SYSTEM
Thermal, Optical, and Electrical Performance Analysis

by

Jawad SARWAR[a], Muhammad R. SHAD[b], Hassan F. KHAN[c], Muhammad TAYYAB[a], Qamar ABBAS[a*], Shahreen AFZAL[a], Muhammad T. MOAVIA[a], and Aiman ASLAM[a]

[a] Department of Mechanical Engineering, University of Engineering and Technology, Lahore, Pakistan
[b] Department of Mechanical Engineering, University of Central Punjab, Lahore, Pakistan
[c] Department of Mechanical Engineering, University of Lahore, Lahore, Pakistan

Original scientific paper
https://doi.org/10.2298/TSCI220917209S

In this work, a validated finite element-based coupled optical, thermal, and electrical model is used to assess the performance of a dual concentrated photovoltaic system thermally regulated using a PCM for the environmental conditions of Lahore, Pakistan. Thermal management of the system is achieved using a selected PCM. That has a melting temperature of 53-56 °C, a thermal conductivity of 19 W/mK, and heat of fusion of 220 kJ/kg. Thermal regulation and power output of the system are analyzed for a clear day of six months of a year. It is found that the maximum temperature of the upper PV cell is ~80 °C while for the bottom PV cell is ~82 °C in July. The percentage power gain obtained after the addition of an upper concentrated PV cell is ~17.9%. The maximum and minimum power of the system is found to be 0.079 kWh/day/m^2 and 0.041 kWh/day/m^2 in May and November, respectively.

Key words: *compound parabolic concentrator, parabolic trough concentrator, concentrated photovoltaics, PCM, output power*

Introduction

Conventional energy has wreaked havoc on the environment in several aspects, including GHG emissions and global warming. It is because of this reason that conventional energy is being replaced by renewable energy. Solar energy is the most widely used renewable energy resource for electric power generation. The PV cells turn irradiance into electrical energy through the PV effect. However, the conversion efficiency of PV cells is limited and even the best-efficiency silicon cell converts 21.2-27.6% of irradiance to electricity, and the rest is dissipated as heat [1].

The output power of PV cells can be enhanced using concentrated photovoltaic (CPV) systems. These systems use optical concentrators to concentrate the irradiance on a smaller area, thereby, resulting in reduced PV cell area and higher electrical output power as compared to a conventional non-CPV systems [2]. However, the high incident irradiance increases the PV cell temperature, concomitantly decreasing its solar-to-electrical conversion efficiency

* Corresponding author, e-mail: 2017me6@student.uet.edu.pk

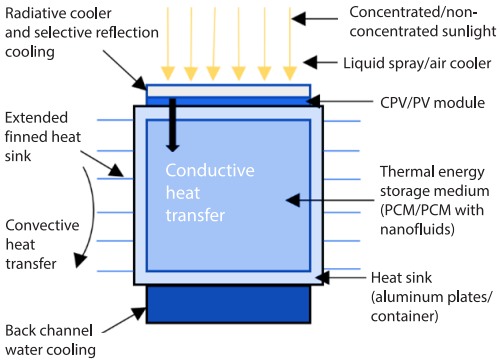

Figure 1. Different thermal management approaches

[3]. Hence thermal management either active or passive is required depending upon the concentration ratio (CR) of the system. Different active and passive approaches are illustrated in fig. 1 and the electrical, η_e, and thermal, η_{th}, efficiency obtained from these approaches are tabulated in tab. 1.

An analysis of the optical performance of the solar power parabolic trough collector system with and without a secondary reflector has been carried out. A secondary reflector in the system increased the optical efficiency by 20% over a conventional collector at a solar incidence angle [9]. In another work, a compound parabolic concentrator (CPC) was modeled and analyzed experimentally on a thermoelectric module. It was observed that the system can generate enough power to lighten up small appliances along with the dissipated heat for additional uses [10]. A feasibility study of the CPV system was carried out by Kamath *et al*. in [11] for the weather condition of India and achieved the system's efficiency of 30%.

Table 1. Thermal management approaches

Thermal management technique	Type	CR	η_e [%]	η_{th} [%]	Reference
Micro-channel heat sink	Active	5	16.8	66.5	[4]
		20	13.2	70.3	
Water cooled	Active	–	15	50	[5]
PCM	Passive	25	7.8	46.6	[6]
Nanofluid	Passive	–	6.6	46.84	[7]
PCM + nanoparticles	Passive	20	8	-	[8]

The benefit of dissipating heat passively is that it does not require any external input energy to operate. Among passive techniques, thermal regulation using a PCM is a useful technique due to its thermal energy storage and efficient thermal regulation of PV and CPV systems [12]. The stored energy reduces the temperature of a PV cell and enables the utilization of thermal energy on demand asynchronously.

The effect of micro-channels with porous media and nanofluids was analyzed for a CPV system. The results demonstrated a 17% reduction in the temperature of the system with the micro-channel and found this technique 30% more efficient than conventional cooling methods [13]. Studies have shown that incorporating a PCM behind a PV system can increase yearly power output by 5.9% when compared to a conventional PV system [14]. The power output of CPV with PCM was found to be 27% higher and its efficiency was 22% higher than the CPV without PCM under typical operating conditions with CR 3 [15].

The performance of a CPV system with RT47 as PCM was analyzed for the weather conditions of Doha, Qatar with CR of 25 [16]. It was observed that the PCM maintained the temperature of the PV cell below 85 °C for all months of a year. In a building-integrated CPV system combined with a PCM heat sink, the temperature of the system was regulated below 78 °C with passive cooling while the temperature was under 43 °C in active cool-

ing with uniform distribution at five suns concentration [17]. The thermal performance of a CPV employing PCM laden with graphene nanoplatelets depicted a 7% and 6% increase in power output and efficiency, respectively for 0.5% volume concentration of *n*PCM at CR = 5 [18].

The power output of PV cells can also be enhanced using bifacial photovoltaic (bPV) cells. The output power of these cells is higher than conventional PV cells because they collect photons from the incident as well as albedo radiation that is reaching both sides of a solar panel. In comparison a conventional PV cell, the bPV cell performed 2% better [19]. The CPV systems have also utilized these cells, but only at low CR due to the lack of thermal management. To overcome this issue of thermal management of the concentrated bPV, a CPV system was presented by Sarwar *et al.* [16] that is similar in working to bPV. The CPV system consists of an aluminum container enclosing PCM and two mono facial PV cells, one at the top surface of the container for non-concentrated sunlight and the other at the bottom for concentrated sunlight.

In this work, the configuration presented by the authors in [16] is modified in such a way that the upper non-CPV cell of the system is replaced with a concentrating one. Two cells are being used at a time, one at the upper and the other at the bottom of the aluminum container. The reduction in the cell area makes the system inexpensive as less material will be required along with the increased power output. The new configuration consists of an aluminum container, encapsulating the PCM having a melting temperature of 53-56 °C, a thermal conductivity of 19 W/mK, and heat of fusion of 220 kJ/kg. The CPV cells are attached to the upper and bottom sides of the aluminum container. The upper cell is concentrated using a non-ideal CPC while the bottom is concentrated using a non-ideal parabolic trough concentrator (PTC) having CR of ~5.5 and ~18.4, respectively. Optical and thermal analysis of the new configuration is carried out to investigate the performance of the system. Moreover, the power output of the system is determined for each month of the year.

Material and methods

Physical model

The non-ideal PTC and non-ideal CPC in this study are designed using the segment division method in which the parabolic curves are divided into straight segments of equal or unequal length depending upon the type of concentrator [20]. The lower part of the system consists of a receiver and a non-ideal PTC whereas the upper part of the system consists of a receiver and a non-ideal CPC. The receivers in the system are PV cells which are labelled as UCPV and BCPV in fig. 2(b) and the whole system is using single axis tracking. The temperature of both PV cells is passively regulated using a PCM. Two mono-facial crystalline silicon PV cells are used in the system.

The non-ideal PTC is modeled by altering the ideal geometry of parabolic curve into straight segments of equal length depending upon the width of the concentrator and non-ideal CPC is modeled by altering the ideal geometry of the parabolic curves into straight segments of increasing length depending upon its projection length on the PV cell. For the non-ideal PTC, the segment length is taken to be 16 mm, which is equal to the width of the absorber surface. The width of the PV cell is 15 mm whereas the width of the absorber surface is kept 16 mm. Non-ideal CPC is also designed on the same principle, but the length of each segment is determined based on its projected length on the absorber plane as discussed earlier. Figure 2(a) shows different design parameters of dual concentrated parameters of *d*CPVPCM like aperture area W_{CPC} and W_{PTC} of both concentrators, cell width, d, CPC height, h, non-ideal PTC focal

length, *f,* and the gap between non-ideal PTC profile, *D*. The schematic illustration of the system is shown in fig. 2 (b).

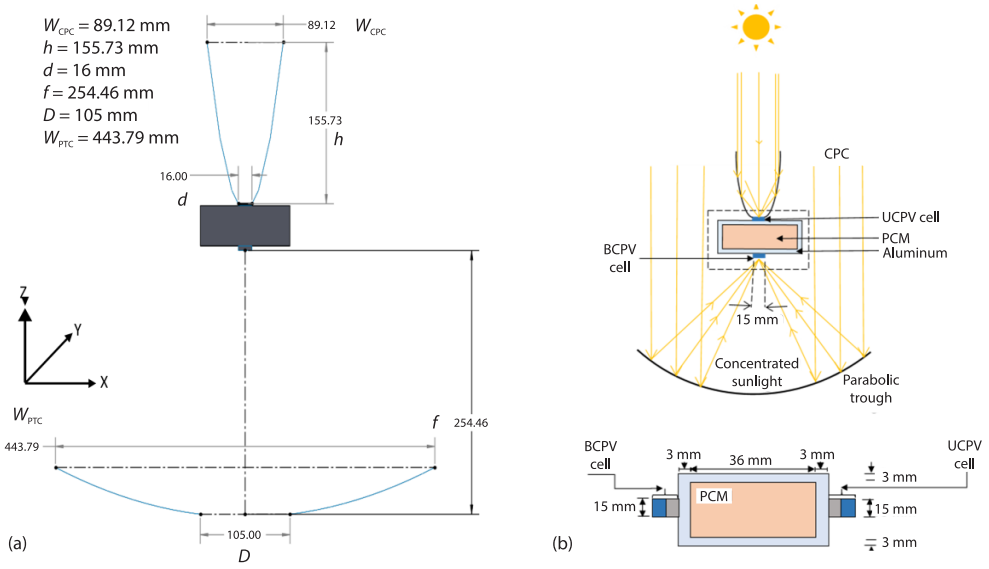

Figure 2. (a) Geometrical parameters of the system and (b) schematic illustration of the system (not to scale)

The model employs two polycrystalline silicon PV cells having a width of 15 mm each, two concentrators, and a footprint of 1 m^2. Both PV cells are attached to an aluminum container, one at the top surface and the other at the bottom surface. Thermal regulation is passively achieved using the PCM, which is encapsulated in a 0.105 m × 0.042 m × 0.015 m aluminum container that acts as a heat sink. A single-axis tracking system is assumed with the concentrator.

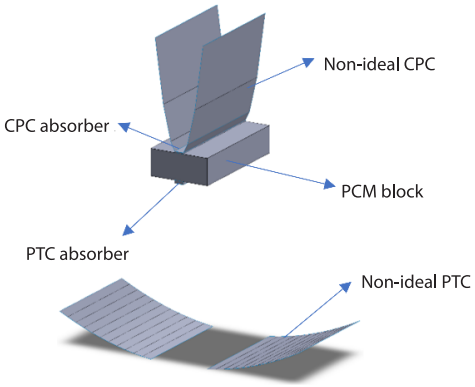

Figure 3. Design model Imported in TracePro

For the optical analysis of the non-ideal CPC and PTC, the computer-aided design designed in SOLIDWORKS was imported into TracePro (Optical design software) [21] for ray tracing analysis. The modeled design is shown in fig. 3. After importing the design in TracePro, reflective and absorptive properties were assigned to the concentrators and the PV cells, respectively. The simulation was performed for 30 million rays so that the convergence of the solution the exact values can be obtained thus providing more accurate results. TracePro takes into account the refraction, reflection, transmission, and absorption properties of the material as a function of the incident angle of the irradiance, therefore, no separate incident angle modifier studies are required. The irradiance value used was 1000 W/m^2.

The bottom PV cell, the top PV cell, and the system will be referred as BCPV, UCPV, and *d*CPVPCM, respectively in the subsequent text. A validated finite element-based coupled optical, thermal, and electrical model is used to assess the performance of the *d*CPVPCM for the

environmental conditions of Lahore, Pakistan (latitude: 31.6946 °N and longitude: 74.2441°E). The incident beam irradiance, ambient temperature, and wind speed data are obtained from the World Bank and a clear day of each month is selected for the analysis. The data has also been used by authors elsewhere [22]. The variation of the weather data with time is shown in fig. 4.

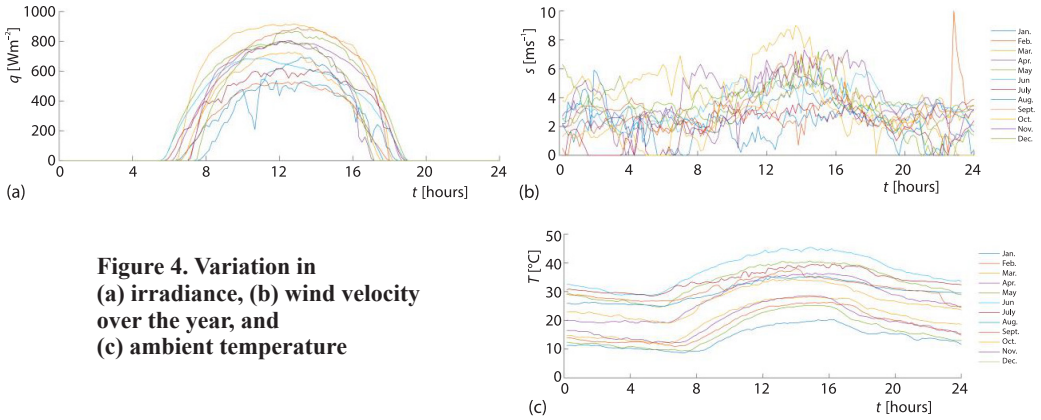

Figure 4. Variation in (a) irradiance, (b) wind velocity over the year, and (c) ambient temperature

Theoretical model

A coupled thermal, optical, and electrical model is used to examine the effect of ambient temperature and the thermophysical properties of PCM on the power output of the *d*CPVPCM system. Fresnel lens equation is used for developing the optical model that determines the reflectivity and absorptivity losses through the glass covering of the PV cell. The thermal and electrical behavior of the system is determined using the thermophysical properties of the selected PCM. For the thermal model, a 2-D differential heat diffusion equation is used to investigate the convective and radiative heat losses. At the PV surface, heat flux represented as incident irradiance is used as a boundary condition. The fundamental eqs. (2) and (3) related to convection and radiation boundary conditions are reported by the author [23]. The detailed thermal model is presented by authors elsewhere [23] and the weak formulation of energy balance equation obtained from eqs. (1)-(3) is given in eq. (4):

$$\rho_o c \frac{\partial T}{\partial t} - \left[\frac{\partial T}{\partial x_i} \left(k_{ij} \frac{\partial T}{\partial x_j} \right) \right] = 0 \tag{1}$$

$$\mathbf{H} = h_c A \Delta T \tag{2}$$

$$\mathbf{R} = h_r A \Delta T \tag{3}$$

$$\int_{\Omega} \delta T \rho_o c \frac{\partial T}{\partial t} \partial\Omega + \int_{\Omega} \left[k_{11} \frac{\partial \delta T}{\partial x_1} \left(\frac{\partial T}{\partial x_1} \right) + k_{22} \frac{\partial \delta T}{\partial x_2} \left(\frac{\partial T}{\partial x_2} \right) \right] \partial\Omega - \int_{r} \delta T \mathbf{q} \partial A + \int_{r} \delta T \left(\mathbf{H} + \mathbf{R} \right) \partial A = 0 \tag{4}$$

where ρ_o is the density, c – the heat capacity, k – the thermal conductivity, T – the temperature, t – time, Ω – the domain, x_i and x_j are unit vectors, δT – the test function, and h_c and h_r are convective and resistive heat loss coefficients, respectively. The matrix form of energy balance equation:

$$\mathbf{M}\dot{T} + \mathbf{K}T - \mathbf{q} + \left(\mathbf{H} + \mathbf{R} \right) T = 0 \tag{5}$$

where **M** is the mass matrix, **q** – the irradiance matrix or boundary flux matrix, the temperature is represented by T, and its time derivative is $\dot{T}$. The **K** is the conductivity, **H** – the convection, and **R** – the radiation matrix. The coupled optical and electrical model is shown [14]:

$$\begin{aligned} q_o &= (1-\rho-\alpha)q_i \\ q_e &= \left[\eta_{ei\text{-STC}} + \mu(T-T_a)\right]q_o \\ q &= q_o - q_e \end{aligned} \tag{6}$$

where $\eta_{ei\text{–STC}}$ is the efficiency of the PV cell at standard test conditions, μ – the temperature coefficient of the power output, T_α – the ambient temperature, q_o – the effective irradiance available after all the losses, and q_i – the incident flux. At every time step, irradiance, ambient temperature, and wind speed are given as input parameters and for that, the values of heat generated, optical losses, and electrical conversion are updated for each step. These values are then used in the thermal model to evaluate the temperature of the PV cells for each time step. The total amount of energy absorbed by the PCM, Q_s, is determined using:

$$Q_s = \begin{cases} mc_s(T-T_1) & T < T_1 \\ mc_s(T_1-T) + mc_e(T-T_1) & T_1 \le T \le T_2 \\ mc_s(T_1-T) + mc_e(T-T_1) + mc_l(T-T_2) & T > T_2 \end{cases} \tag{7}$$

where T_1 and T_2 are the solidus and liquidus temperatures of PCM, respectively. The electrical power output is determined using the five-parameter model as described in detail in [24]. The equation of five- parameter model relating current, and voltage is given:

$$I = I_{\text{pv}} - I_o\left[\exp\left(\frac{V+R_sI}{V_t a}\right)\right] - \frac{V+R_sI}{R_p} \tag{8}$$

The parameters are photocurrent I_{pv}, reverse saturation diode current I_a, shunt and series resistances R_p and R_{s} and diode ideality factor a. The power gain of the system with total power, P_T and initial power P_i is calculated using eq. (9) and the material properties used in this analysis are tabulated in tab. 2:

$$P_{\text{gain}} = \frac{P_T - P_i}{P_i} \tag{9}$$

Table 2. Material properties

Thermophysical properties					
Material	T_m [°C]	H [kJkg^{-}1]	k [Wm^{-1}K^{-1}]	ρ_o [kgm^{-3}]	c_o (s, l) [kJkg^{-1}K^{-1}]
PCM	53-56	220	19	880	2
Aluminum	–	–	211	2675	0.9
PV	–	–	125.4	2205	0.8
Electrical properties of PV cell					
V_{oc} [V]	I_{sc} [A]	V_{mp} [V]	I_{mp} [A]	K_v [%K^{-1}]	K_I [%K^{-1}]
32.9	8.21	26.3	7.61	–0.1	0.0032
Optical properties					
PV	n	K [m^{-1}]		x [m]	
	4	4710		$5 \cdot 10^{-4}$	

Results and discussion

Optical analysis of non-ideal concentrator

The design of the half profile of the non-ideal PTC and CPC is shown in fig. 5. The flux distribution profile along the PV cell for both concentrators is shown in fig. 6 which depicts that the distribution of the flux is uniform from –7.5 mm to 7.5 mm on the PV cell surface. The value of irradiance absorbed by BCPV drops from 18423-789.6 W/m^2 to for –8 mm to –7.5 mm, and 7.5-8 mm in the horizontal and vertical direction. The geometrical efficiency of PTC is about 89% and the geometric loss comes out to be about 11% due to its non-ideal geometry. The irradiance absorbed by UCPV drops from 5465-2006.1 W/m^2 for 8 mm to –7.5 mm and 7.5-8 mm in horizontal and vertical directions.

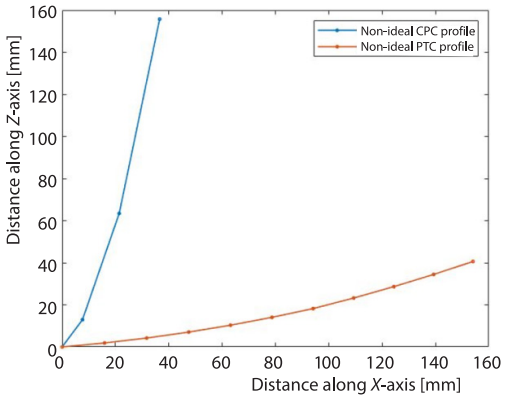

Figure 5. Half profile of non-ideal CPC and PTC

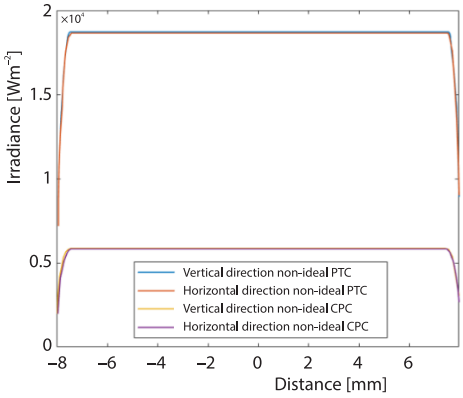

Figure 6. Flux distribution profile for CPC and PTC

The geometrical efficiency of CPC is about 66.7% and the geometric loss comes out to be about 33.3% due to its non-ideal geometry. While fig. 7 shows the total absorbed flux along the PV cell for both concentrators. A non-ideal PTC concentrates uniformly distributed irradiance (~18.4×) on the bottom PV cell shown in fig. 7(a) while the non-ideal CPC concentrates uniformly distributed ~5.5× irradiance on the top PV cell shown in fig. 7(b).

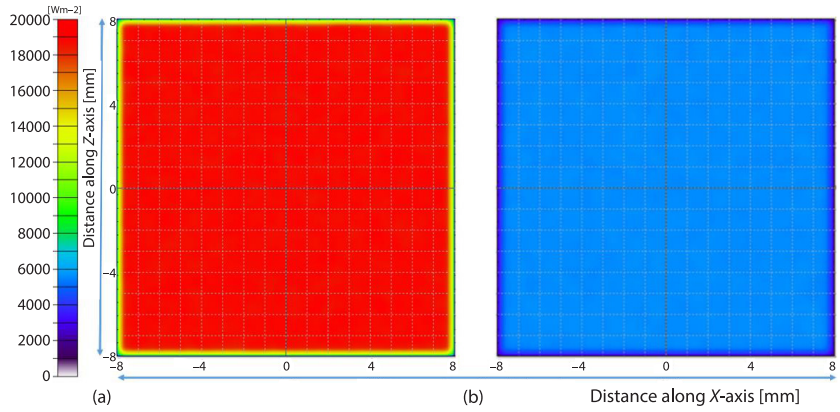

Figure 7. Irradiance map for (a) non-ideal PTC and (b) non-ideal CPC

Thermal regulation

To analyze the thermal management of the system, the comparison of maximum and average temperatures of UCPV and BCPV is carried out for six months of a year. The variation of temperature of UCPV and BCPV throughout the day for selected months of the year is shown in fig. 8(a). The temperature is high during the middle of the day as there is more irradiance available to UCPV and BCPV for a longer duration.

The results for the comparison of peak temperatures of UCPV and BCPV are plotted in fig. 8(b). The peak temperature of BCPV consistently stays higher than the peak temperature of UCPV because non-ideal PTC with higher CR is concentrating irradiance on BCPV. The lowest peak temperature for BCPV and UCPV is in November as the irradiance and ambient temperature in this month are the lowest among all months of the year.

The results for the comparison of average temperatures of UCPV and BCPV are plotted in fig. 8(c). The average temperature of BCPV consistently stays higher or almost equal to the average temperature of UCPV. The trend line in figs. 8(b) and 8(c) is showing that the peak temperature and average temperature for UCPV and BCPV is increasing during the early months of the year and have the highest values during the midsummer because of higher irradiance with longer duration and then the temperature for UCPV and BCPV is decreasing at the end of the year. The variation of temperature from BCPV to UCPV including the PCM and aluminum container at different hours of the day for July is shown in figs. 8(d)-8(f). Early in the day, at 9:00 a. m. and 10:00 a. m., the center of the PCM is at 53.8 °C and 55.1 °C, respectively, while the BCPV and UCPV are at higher temperatures because their surfaces are absorbing irradiance and begin to charge thermal energy inside PCM as shown in fig. 8(d). This resulted in the heating of the PCM and then at midday, at 11:00 a. m. and 12:00 p. m., the temperature of PCM reached 59 °C and 77.8 °C, respectively which is the indication that PCM has absorbed heat and melted to regulate the cell temperatures as depicted in fig. 8(e). The temperature of PCM has again decreased in the afternoon hours, at 1:00 p. m. and 2:00 p. m., to 76.3 °C and 73.1 °C, respectively which is indicating that the PCM has started releasing its absorbed heat for regeneration as shown in fig. 8(f).

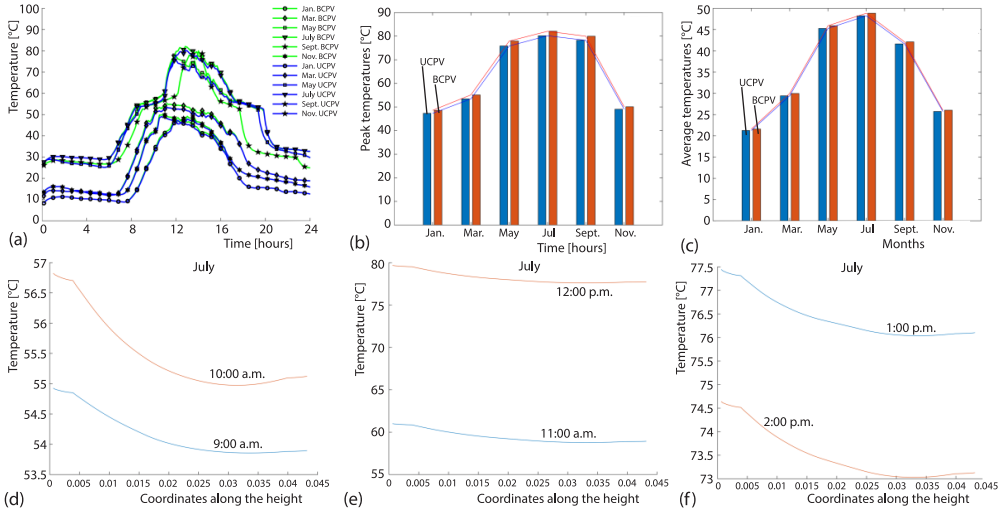

Figure 8. (a) Variation of temperature of UCPV and BCPV over the day, (b) comparison of peak temperature of UCPV and BCPV, (c) comparison of average temperature of UCPV and BCPV, and (d) and (f) the melting behavior of PCM over the day

Output power

Further studies are carried out to calculate the power output of BCPV and UCPV of *d*CPVPCM and the power gain obtained after adding UCPV in the *d*CPVPCM system. The comparison of power output per day of UCPV and BCPV is evaluated for six months of a year and the results are shown in fig. 9(a). The power output from BCPV is almost ~3% higher than UCPV due to the higher geometric CR of non-ideal PTC compared to non-ideal CPC. The maximum power of UCPV is obtained for May *i.e.*, 0.017 kWh/day/m^2.

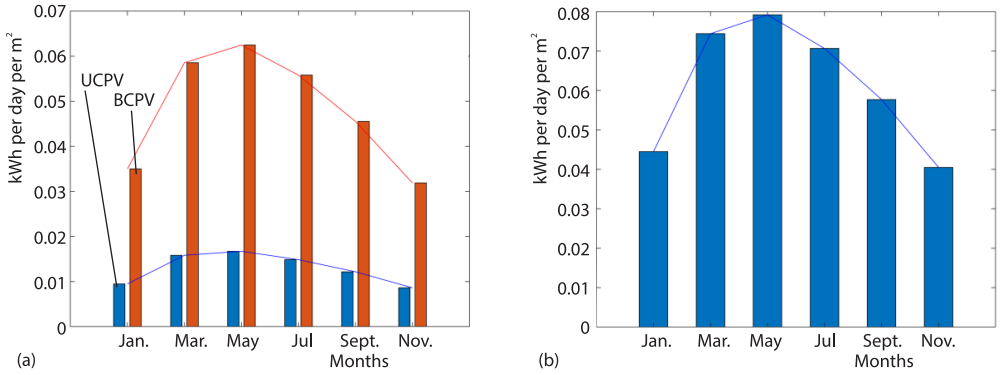

Figure 9. (a) Comparison of output power of upper PV cell and bottom PV cell and (b) output power of the system

The maximum power of BCPV is obtained for May *i.e.*, 0.062 kWh/day/m^2. During summer months when there is increased irradiance available to BCPV and UCPV for longer durations, the power output of the system in turn increases. The total power output per day of the *d*CPVPCM is also evaluated for six months of a year and the results are shown in fig. 9(b). The maximum power of *d*CPVPCM is obtained for May *i.e.*, 0.079 kWh/day/m^2. The total power obtained is also showing the same trend as of UCPV and BCPV as it's the summation of both. The percentage power gain obtained after the addition of UCPV is ~17.9 %.

Conclusions

In this work, a finite element based coupled optical, thermal, and electrical model is used to evaluate the thermal regulation and the power output of a dual CPV system. The system comprised of an aluminum container encapsulating PCM with two polycrystalline silicon cells attached at the top and bottom of the container. Both cells are concentrated using CPC and PTC. Following are the conclusions obtained from this study, are as follows.

- Both non-ideal CPC and non-ideal PTC provided uniform flux distribution and CR of ~5.5 and ~18.4, respectively.
- The temperature of the UCPV and BCPV remained below 83 °C for six months of the year which makes the selected PCM suitable for the current configuration.
- The power output of the system is found to be highest in May *i.e.*, 0.079 kWh/day/m^2.

The proposed system is suitable for achieving higher electrical output because of the utilization of two concentrated cells in a single system. However, further studies would be done to investigate the reduction of temperatures of UCPV and BCPV by using a larger volume of PCM, the utilization of stored energy of PCM for water heating, and optimization of the system in terms of geometry and materials. For the simplicity of current studies, wind loading is not considered for the system, however, it is one of the primary horizontal loads that act on

structures that are exposed to a direct environment thus limitations due to wind loadings on the height of CPC would be considered in future analysis.

Nomenclature

a – diode ideality factor
c – heat capacity, [JK^{-1}]
D – gap between non-Ideal parabolic trough concentrator profiles, [mm]
d – cell width, [m]
f – non-ideal PTC focal length, [m]
$\mathbf{H}$ – convection matrix
h – CPC height, [m]
h_c – convection heat transfer coefficient, [Wm^{-2}K^{-1}]
h_r – resistive heat transfer coefficient, [Wm^{-2}K^{-1}]
I_o – reverse saturation diode current, [A]
I_{pv} – photo current, [A]
k – thermal conductivity, [Wm^{-1}K^{-1}]
$\mathbf{K}$ – conduction matrix
$\mathbf{M}$ – mass matrix
$\mathbf{q}$ – irradiance matrix or boundary flux matrix, [Wm^{-2}]
q_i – incident flux, [Wm^{-2}]
q_o – effective irradiance available after all the losses, [Wm^{-2}]
$\mathbf{R}$ – radiation matrix
R_p – shunt resistance, [Ω]
R_s – series resistance, [Ω]
T – temperature, [K]
T_α – ambient temperature, [K]
$\dot{T}$ – time derivative of temperature
T_1 – solidus temperature, [K]
T_2 – liquidus temperature, [K]
t – time
V_z – mean wind speed, [ms^{-1}]
W_{CPC} – aperture of compound parabolic concentrator, [mm]
W_{PTC} – aperture of parabolic trough concentrator, [mm]

Greek symbols

α – absorptivity
η_e – electrical efficiency
η_{ei} – efficiency of the PV cell
η_{th} – thermal efficiency
μ – temperature coefficient of the power output
ρ – reflectivity
ρ_o – dynamic density of air
Ω – domain

Acronyms

BCPV – bottom concentrated photovoltaic
bPV – bifacial photovoltaic
CPC – compound parabolic concentrator
CPV – concentrated photovoltaic
CPVPCM – concentrated photovoltaic system with phase change material
CR – concentration ratio
PTC – parabolic trough concentrator
UCPV – upper concentrated photovoltaic

References

[1] ***, NREL. Best Research-Cell Efficiency Chart. Available: https://www.nrel.gov/pv/cell-efficiency.html, 2021
[2] Hasan, A., *et al*., Concentrated Photovoltaic: A Review of Thermal Aspects, Challenges and Opportunities, *Renewable and Sustainable Energy Reviews*, *94* (2018), Oct., pp. 835-852
[3] Jaaz, A. H., *et al*., Outdoor Performance Analysis of a Photovoltaic Thermal (PVT) Collector with Jet Impingement and Compound Parabolic Concentrator (CPC), *Materials*, *10* (2017), 8
[4] Elqady, H. I., *et al*., Concentrator Photovoltaic Thermal Management Using a New Design of Double-Layer Micro-Channel Heat Sink, *Solar Energy*, *220* (2021), May, pp. 552-570
[5] Hazami, M., *et al*., Energetic and Exergetic Performances Analysis of a PV/T (Photovoltaic Thermal) Solar System Tested and Simulated under to Tunisian (North Africa) Climatic Conditions, *Energy*, *107* (2016), July, pp. 78-94
[6] Sarwar, J., *et al*., Performance Analysis and Comparison of a Concentrated Photovoltaic System with Different Phase Change Materials, *Energie*s, *14* (2021), 10, 291
[7] Bellos, E., *et al*., Investigation of a Nanofluid-Based Concentrating Thermal Photovoltaic with a Parabolic Reflector, *Energy Conversion Management, 180* (2019), Jan., pp. 171-182
[8] Zarma, I., *et al*., Enhancing the Performance of Concentrator Photovoltaic Systems Using Nanoparticle-Phase Change Material Heat Sinks, *Energy Conversion and Management, 179* (2019), Jan., pp. 229-242
[9] Subramaniyan, C., *et al.*, Investigation on the Optical Design and Performance of a Single-Axis-Tracking Solar Parabolic trough Collector with a Secondary Reflector, *Sustainability*, *13* (2021), 17, 9918

[10] Mgbemene, C. A., *et al*., Electricity Generation from a Compound Parabolic Concentrator Coupled to a Thermoelectric Module, *Journal Sol. Energy Eng*., *52* (2014), Dec., pp. 150-158
[11] Kamath, H. G., *et al*., The Potential for Concentrator Photovoltaics: A Feasibility Study in India, *Progress in Photovoltaics*, *27* (2019), 4, pp. 316-327
[12] Zalba, B., *et al*., Review on Thermal Energy Storage with Phase Change: Materials, Heat Transfer Analysis and Applications, *Applied Thermal Engineering*, *23* (2003), 3, pp. 251-283
[13] Farahani, S. D., *et al*., The Effect of Micro-Channel-Porous Media and Nanofluid on Temperature and Performance of CPV System, *Journal of Thermal Analysis and Calorimetry*, *147* (2022), 14, pp. 7945-7960
[14] Hasan, A., *et al*., Yearly Energy Performance of a Photovoltaic-Phase Change Material (PV-PCM) System in Hot Climate, *Solar Energy*, *146* (2017), Apr., pp. 417-429
[15] Manikandan, S., *et al*., Thermal Management of Low Concentrated Photovoltaic Module with Phase Change Material, *Journal of Cleaner Production*, *219* (2019), May, pp. 359-367
[16] Sarwar, J., *et al*., Comparative Analysis of a Novel Low Concentration Dual Photovoltaic/Phase Change Material System with a Non-Concentrator Photovoltaic System, *Thermal Science*, *25* (2021), 2A, pp. 1161-1170
[17] Rahmanian, S., *et al*., Nanofluid-PCM Heat Sink for Building Integrated Concentrated Photovoltaic with Thermal Energy Storage and Recovery Capability, *Sustainable Energy Technologies and Assessments*, 46 (2021), 101223
[18] Sivashankar, M., *et al*., Performance Improvement in Concentrated Photovoltaics Using Nanoenhanced Phase Change Material with Graphene Nanoplatelets, *Energy*, *208* (2020), 118408
[19] Hasan, A., A New Performance Assessment Methodology of Bifacial Photovoltaic Solar Panels for Offshore Applications, *Energy Conversion Management*, *220* (2020), 112972
[20] Sarwar, J., *et al*., Novel Method to Design Non-Ideal Parabolic Dish Concentrator for Concentrated Photovoltaic Application; Its Theoratical Analysis and Experimental Characterisation for Design Validation, *Proceeddings*, 28th European Photovoltaic Solar Energy Conference and Exhibition, Paris, France, 2013, pp. 632-635
[21] Sarwar, J., *et al*., Comparative Analysis of a Novel Low Concentration Dual Photovoltaic/Phase Change Material System with a Non-Concentrator Photovoltaic System, *Thermal Science*, *25* (2021), 2A, pp. 1161-1170
[22] Hasnain, A., *et al*., Thermal and Electrical Performance Analysis of a Novel Medium Concentration Dual Photovoltaic System for Different Phase Change Materials, American Society of Mechanical Engineers, *Proceedings*, ASME International Mechanical Engineering Congress and Exposition, 2020, Vol. 84560, V008T08A011
[23] Sarwar, J., *et al*., Effect of the Phase Change Material's Melting Point on the Thermal Behaviour of a Concentrated Photovoltaic System in a Tropical Dry Climate, *Proceedings*, ISES Conference Proceedings, San Francisco, Cal., USA, 2016
[24] Villalva, M. G., *et al.*, Comprehensive Approach to Modelling and Simulation of Photovoltaic Arrays, *IEEE Transactions on Power Electronics*, *24* (2009), 5, pp. 1198-1208

Paper submitted: September 17, 2022
Paper revised: October 20, 2022
Paper accepted: November 2, 2022